DELPHI Collaboration DELPHI 2003-004 CONF 627
March 13, 2003

Search for a fermiophobic Higgs at LEP 2

S. Andringa, M. Espírito Santo, P. Gonçalves,
A. Onofre, M. Pimenta and B. Tomé
LIP-IST, Av. Elias Garcia, 14, 1, P-1000 Lisboa, Portugal

Abstract

Higgs bosons decaying into two photons were searched for in the data collected by the DELPHI detector at centre-of-mass energies between 183 GeV and 209 GeV, corresponding to a total integrated luminosity of nearly 650 pb^{-1}. No evidence for new phenomena was found, and limits were set on the cross-section for h^0Z^0 production with subsequent Higgs boson decays to photons, and on h^0A^0 production. These results were used to the exclude regions in the parameter space in fermiophobic scenarios of Two Higgs Doublet Models.

Contribution to Winter Conferences 2003

1 Introduction

Within the Standard Model (SM), the decay of the Higgs boson to photons proceeds via loops of heavy charged particles, namely $W^{\pm}$ bosons and top-quarks, and the corresponding branching ratio (BR) is below 0.1%. The experimental signature of a two-photon resonance is, on the other hand, clear enough to make this decay mode one of the main channels for Higgs searches at hadron colliders.

At LEP, this search is motivated by extensions of the SM. In fact, many of the proposed models may enhance this BR, either by enlarging the $H\gamma\gamma$ coupling [1] or by reducing the coupling of the Higgs to fermions [2]. Based on the Higgs-strahlung (h^0Z^0 production) mechanism, the search for two photons produced with a fermion pair can give a clear indication of new physics.

In this paper we investigate the fermiophobic scenario of Two Higgs Doublets Models (2HDM) [2], in which the lightest scalar Higgs boson decays to photons and can be produced together with a Z^0 or a CP-odd scalar Higgs boson A^0. The results reported here update those obtained with lower integrated luminosity and at lower centre-of-mass energies [3]. The search for h^0Z^0 now includes the leptonic decays of the Z^0 and improved analyses for the other final states; all the hadronic final states with photons were also reanalysed, profiting from improved selections but also from a more accurate description of the main SM background.

The results on h^0Z^0 production with $h^0 \to \gamma\gamma$ have been interpreted in several frameworks: previous analyses of DELPHI data can be found in [3] and [4] and results from the other LEP experiments can be found in [5]. In all cases, h^0Z^0 production with subsequent $h^0 \to \gamma\gamma$ decay, has been used as a benchmark for the search for particles with SM Higgs-like couplings to bosons but no couplings to fermions.

The Higgs decay modes analysed in this paper are $h^0 \to \gamma\gamma$ and $A^0 \to b\bar{b}$ or $A^0 \to h^0Z^0$. However, we consider also results for $h^0 \to A^0A^0$ and for long-lived A^0, as described in [3]. In particular, for 6-fermion final states, common to a variety of 2HDM, the analysis from [6] is used.

2 The 2HDM fermiophobic scenario

Two Higgs Doublets Models without explicit CP violation are characterized by five physical Higgs bosons: two neutral CP-even bosons (h^0 and H^0), two charged bosons ($H^{\pm}$) and one neutral CP-odd boson (A^0). Together with the masses, the important parameters describing 2HDMs are the mixing angle in the neutral CP-even sector (α) and the ratio of the vacuum expectation values of the two Higgs doublets ($\tan\beta$).

The couplings of the Higgs doublets to fermions could be realized in different ways, one possibility is that only one of the doublets couples to fermions. The coupling of the lightest CP-even boson to a fermion pair is then proportional to $\cos\alpha$. If $\alpha = \pi/2$ this coupling vanishes and h^0 becomes a fermiophobic Higgs [2]: it will decay to pairs of other Higgs bosons or massive gauge bosons when kinematically allowed, or to two photons in a large region of the parameter space.

In the general 2HDM, the main mechanisms for the production of neutral Higgs bosons at LEP are $e^+e^- \to h^0Z^0$ and $e^+e^- \to h^0A^0$, both proceeding via Z^0 exchange. The two processes have complementary cross-sections proportional to $\sin^2\delta$ and $\cos^2\delta$, respectively,

where $\delta = \alpha - \beta$. The $\sin\delta$ factor rescales the $h^0 Z^0 Z^0$ vertex with respect to the SM one.

It must be noticed that there are two different seven parameter potentials which conserve CP [2] (they are referred to as Potential A and B). The choice of the potential does not affect the Higgs interactions with gauge bosons or fermions but leads to different Higgs-Higgs couplings and thus different phenomenologies. In particular, the decay width of $h^0 \to \gamma\gamma$, for which the $H^\pm$ loop (together with the $W^\pm$ loop) has a fundamental contribution, can be dramatically changed.

For potential A, the branching ratio of the lightest scalar Higgs, h^0, to two photons, BR($h^0 \to \gamma\gamma$), depends on M_{h^0} and mildly on $\sin^2\delta$. Provided that the decay to H^+H^- is kinematically closed (as guaranteed by the experimental limit $M_{H^\pm} > 74$ GeV/c^2 [7]) and that $M_{H^0} \sim 1$ TeV/c^2, the lower limit for this BR (obtained when $\sin^2\delta = 1$) is equal to the one obtained with SM couplings to bosons and no couplings to fermions. For Potential B, the BR($h^0 \to \gamma\gamma$) depends also on M_{A^0} and $M_{H^\pm}$, and there can be large cancellations between the several loop contributions for some values of these parameters. The tree-level A^0 decays are independent of the potential but depend on M_{A^0}, M_{h^0} and $\sin^2\delta$; for low values of $\sin^2\delta$, also A^0 becomes fermiophobic and thus long-lived.

The low values of $\sin^2\delta$ lead also to different kinematic regions according to the choice of potential. For Potential A they imply low M_{h^0} and for Potential B $M_{h^0} \sim M_{A^0}$.

3 Detector and Data Samples

The DELPHI apparatus and performance are described in detail in [8]; more recent minor changes affected mainly the forward tracking [9]. The most relevant subdetectors for the present analysis were the electromagnetic calorimeters: the High density Projection Chamber (HPC) in the barrel region and the Forward ElectroMagnetic Calorimeter (FEMC) in the endcaps. The FEMC covered polar angles[1] between 11° and 35°, the HPC covered polar angles above 42° and consisted of 144 modules, with azimuthal intermodular divisions at $mod(\phi, 15°)$=7.5°, in which the detection of photons could be complemented by the use of the Hadronic CALorimeter (HCAL, covering polar angles down to 11°). The regions in between the FEMC and the HPC were equipped with with hermiticity counters – scintillators covered with lead so that photons could also be tagged there. The DELPHI electromagnetic calorimetry was complemented by the luminosity monitor, STIC, covering the polar angle region between 3° and 11°.

The most relevant tracking devices were the Vertex Detector (VD), the Inner Detector (ID) and the Time Projection Chamber (TPC), covering polar angles above 20°. The tracking system was complemented by the information provided by the Outer Detector (OD) in the barrel and the Forward Chambers A and B (FCA, FCB) in the forward region. The Vertex Detector is crucial for the determination of secondary vertices and the tagging of b-quark jets and, most important for the present analysis, in the discrimination between photons converting inside the tracking system (but after the VD) and charged particles coming from the interaction point.

The analysed data were taken by the DELPHI detector in the LEP runs of 1997 to 2000. The corresponding centre-of-mass energies ($\sqrt{s}$) and integrated luminosities ($\mathcal{L}$) are shown in table 1.

[1] The polar angle θ is defined in relation to the beam axis. In all cases also the complementary value $(180° - \theta)$ is also assumed.

year	1997	1998	1999				2000		
$\sqrt{s}$ (GeV)	182.6	188.6	191.6	195.5	199.6	201.6	205.0	206.5	206.8
$\mathcal{L}$ (pb^{-1})	49.3	153.0	25.1	76.0	82.7	40.2	80.0	59.2	81.8

Table 1: Centre-of-mass energies and integrated luminosities of the analysed samples.

In the year 2000, the centre-of-mass energies ranged from 200 GeV to 209 GeV, with luminosity peaks at 205 GeV and 207 GeV. In the last part of the year, DELPHI suffered from a problem in a section (1/12) of the TPC and, although this does not affect much the present search, these data were analysed separately.

Signal processes were generated according to Pythia 6.1 [10], while the main background processes were generated with KK2f [11] (for $q\bar{q}(\gamma)$), KoralZ [12] (for $\nu\bar{\nu}(\gamma)$ and $l^+l^-(\gamma)$) and Bhwide [13] (for the Bhabha scattering), all of which include a detailed description of the initial state radiation. All the generated data sets at the different centre-of-mass energies were passed through the DELPHI simulation and reconstruction chain; dedicated samples were used to match the data affected by the TPC problem.

4 Event Selection

The analysis of events with isolated photons was done in several steps. First a general selection was applied and isolated photons and leptons were reconstructed.

Only events with visible energy in the polar angle region above 20° greater than $0.2\sqrt{s}$ were accepted (except for the topology with only photons for which this threshold was lowered to $0.1\sqrt{s}$). In addition, all events were required to contain at least one charged or neutral object with energy above 5 GeV in the same polar angle region. This vetoed most of the contamination from "$\gamma\gamma$ interaction" events.

Good charged particle tracks were required to have momentum greater than 0.1 GeV/c and impact parameters below 4 cm in the transverse plane and below 4 cm $/\sin\theta$ in the beam direction; energy deposits in the calorimeters unassociated to charged particle tracks were required to be above 0.3 GeV.

The reconstruction of photons in DELPHI was done is several steps, starting from the showers in the electromagnetic calorimeters. In the barrel, the procedure described in [8] was followed but, in a looser selection, showers close to the HPC divisions were accepted even if they failed the transverse shower profile criteria, and also the longitudinal shower profile criteria for showers with energy above 25 GeV. In the forward region, all STIC energy deposits with polar angle satisfying $\theta < 11°$ were taken to be photon candidates, while, for $\theta > 11°$, an algorithm was used to reduce the effects of the shower development in the detector material in front of the FEMC. Electromagnetic deposits close in space in the FEMC were clustered together and the association with reconstructed charged tracks was used for electron/photon discrimination. Care was taken to exclude those tracks which were likely to come from the development of showers outside the calorimeter. Photons with two associated tracks could be kept in a looser selection, but the tighter selection required that no VD tracks, nor signals from different combinations of other tracking detectors (depending on the shower polar angle) be associated with the electromagnetic deposit. In addition, the ratio between the electromagnetic energy and the total energy was required

to be above 90% in the angular region around the cluster defined by $|\Delta\theta| < 15^\circ$ and $|\Delta\phi| < \min(15^\circ, 6^\circ \cot\theta_{cluster})$, where ϕ is the angle in the plane perpendicular to the beam direction.

The identification of isolated photons started from the candidates defined above and used a double cone centred around the photon axis, as explained below. Only isolated photons with energies above 5 GeV were considered.

The total energy inside a cone of 5° was associated to the photon, while, to ensure isolation, the energy between 5° and 15° was not permitted to exceed 1 GeV. These criteria were relaxed for tightly identified photons. In this case, no further association was done and the angle of the external cone, α, was varied according to the energy of the photon candidate (down to 3° for $E_\gamma > 90$ GeV). The energy limit inside the cone was rescaled with $\sin\alpha/\sin(15^\circ)$. One energetic particle was still accepted inside this cone (and excluded from the energy counting).

For the topology with photons only, no distinction was made between tight and loose photon candidates, and the cones had fixed opening angles of 10° and 12°: at most 5 GeV of total energy were allowed in between the two cones. The energy inside the inner cone was associated to the photon.

The identification of isolated photons in the barrel region required that there was no HPC layer with more than 90% of their electromagnetic energy, while the hadronic energy depositions above 3 GeV should be concentrated in the first layer of the HCAL.

The identification of isolated leptons followed the same double cone criteria. Isolated charged particles associated to signals in the muon chambers, and for which the ratio between the associated energy and the measured momentum was less than 20%, were identified as muons. The separation between electrons and photons converting in the tracking system relied on the information from the VD and its association to isolated charged particles. A VD track element was defined as at least two signals in different layers of the detector, which were associated to an isolated particle if aligned within 3° of its azimuthal direction (10° in the forward region). Isolated charged particle tracks not associated to VD track elements were considered as candidates for photons converted in the tracking system. At most one converted photon candidate was allowed per event, except for the $l^+l^-\gamma\gamma$ topologies where no recovery of converted photons was performed.

5 Search for h^0Z^0 Production

5.1 Two photons and jets

The preselection of this topology required that at least six good charged tracks were present. All selected charged and neutral particles not associated to isolated photons or leptons were clustered into two jets using the DURHAM jet algorithm [14]. Two isolated photons were required in the event, and extra isolated particles were allowed only if their transverse energy with respect to one of the jets was less than 20 GeV.

The main background to this search, indeed irreducible, is $q\bar{q}$ production with two photons coming mainly from initial state radiation: at LEP2, about half of the $q\bar{q}$ events are radiative return events, in which the beam electrons (positrons) radiate highly energetic photons, lowering the effective collision energy ($\sqrt{s'}$) down to M_{Z^0}. Very small contributions from other sources, namely W^+W^- production, are also present.

After the preselection of two identified photons in the event, further requirements on their isolation and polar angle reduced both Initial and Final State Radiation (ISR and FSR) contributions present in all samples. It was required that the most energetic photon had at least 15% of the beam energy, that the minimum transverse energy of the photons with respect to the jets was above 7.5 GeV and the minimum polar angle above 30°.

To improve the resolution on the invariant mass of the photon pair, a kinematic fit imposing energy-momentum conservation and constraining the jet-jet invariant mass to the Z^0 mass was performed according to [15]. The directions and energies of the photons are the main constraints in the fit, but are considerably weaker if the photons are not well contained in the calorimeters. Events in which both photons were reconstructed near calorimeter boundaries were rejected at this stage. A partial χ^2 was constructed as: $\frac{\chi^2_{\gamma\gamma}}{ndof} = \frac{1}{2}\sum_{i=1,2} \frac{(E^{fit}_{\gamma i} - E^{meas}_{\gamma i})^2}{\sigma^2 E^{meas}_{\gamma i}}$, where σ is the relative error on the measured $E^{meas}_{\gamma i}$ from calorimeter resolution studies. It was set to 100% for photons reconstructed in the calorimeter boundaries. If both photons were well contained in the calorimeters, it was required that $\chi^2_{\gamma\gamma}/ndof$ was below 5. If one of the photons was not well contained, the hadronic part had a larger weight and it was the total $\chi^2/ndof$ that was required to be below 5.

At this stage, the non-$q\bar{q}$ background becomes almost negligible. The characteristics of the radiative return events were then used to further reduce the background. In most of these events, the photons are in the forward part of the detector and, usually, one of the photons carries most of the energy necessary to bring the Z boson on-shell ($E_{ret} = \frac{s - {M_{Z^0}}^2}{2\sqrt{s}}$). Only events in which the energy difference between the two photons was lower than $0.70 E_{ret}$ were kept. Figure 1 shows the sum and difference of the two photon energies normalized to the radiative return energy. In the final sample, one of the photons was required to be inside the HPC acceptance.

Selection	Data	Background	$q\bar{q}$	eff_{50}	eff_{100}
2 photons	338	341.5 ±9.5	296.5 ±9.2	60%	60%
no-ISR/FSR	23	22.9 ±0.3	21.2 ±0.3	39%	45%
Z fit	12	12.4 ±0.2	12.3 ±0.2	31%	41%
ΔE	9	8.7 ±0.2	8.6 ±0.2	26%	40%
HPC	9	8.4 ±0.2	8.3 ±0.2	26%	40%

Table 2: $h^0 Z^0 \to \gamma\gamma q\bar{q}$ selection in the year 2000: the evolution of the data sample with the analysis cuts is shown for the full 2000 data set, compared to the total expected background (and the $q\bar{q}$ background) and the efficiencies for Higgs masses of 50 GeV/c^2 and 100 GeV/c^2. The errors on the backgrounds are statistical only. The statistical error on the efficiencies is 1-2%.

Table 2 shows the evolution of the data sample collected in the year 2000, corresponding SM background and efficiencies for two Higgs signals of different masses, with the cuts. The contribution of the irreducible $q\bar{q}(\gamma\gamma)$ background is shown separately. KK2f has a more accurate description of the initial state photon radiation and a better match to the DELPHI data than the previously used generator (Pythia 6.1 in [3]), for example

after the anti ISR/FSR cuts there would be 15.9 events in Pythia compared to 21.2 in KK2f.

The numbers of events selected in all data and simulated samples at the final selection level are shown in table 5. The reconstructed jet-jet invariant masses and the fitted $\gamma\gamma$ masses are also shown in figure 1.

5.2 Two photons and two charged leptons

The preselection of this topology required the presence of two isolated photons and two isolated leptons in events with at most five good charged particle tracks. The most energetic photon was required to have energy greater than $0.1\sqrt{s}$ and the polar angle of the leptons was required to be above 20° (except for the ones identified as muons).

The background processes for these channels include $e^+e^- \to Z^0/\gamma^* \to l^+l^-(\gamma)$ and the t-channel Bhabha scattering, which has a very large cross-section. To reduce the number of events from FSR, the minimum transverse energy of each photon with respect to any of the leptons was required to be greater than 5 GeV. The contribution from ISR, namely from radiative return to the Z^0, was reduced requiring that both photons had polar angles above 30°, that there was at least one photon in the HPC and imposing that the difference between the energies of the two photons was below $0.7E_{ret}$.

A kinematic fit imposing energy-momentum conservation and using the measured directions of the four particles in the event was performed. Events were accepted only if the partial $\chi^2/ndof$ associated to the leptons or to the photons was below 10. Finally, since the lepton pair should originate from a Z^0 decay, only events for which the fitted di-lepton invariant mass was between 60 and 120 GeV/c^2 were kept.

Table 3 presents the number of events selected in the year 2000 data and the corresponding SM background expectations, at each selection level, together with the efficiencies for two Higgs masses. The selection efficiencies for the different leptonic decays of the Z^0 vary between 13% for $\tau^+\tau^-$ and 38% for $\mu^+\mu^-$ for a Higgs mass of 100 GeV/c^2. The lepton identification was not taken into account in the limit setting. The final invariant mass spectra are shown in figure 2, and the corresponding numbers of events selected in each data set are given in table 5.

Selection	Data	Background	eff_{50}	eff_{100}
2 photons	24	28.8 $\pm$1.1	36%	36%
no-ISR/FSR	5	5.3 $\pm$0.5	22%	31%
fit + M_{Z^0}	0	1.5 $\pm$0.2	17%	27%

Table 3: $h^0Z^0 \to \gamma\gamma l^+l^-$ selection in the year 2000: the evolution of the data sample with the analysis cuts is shown together with the total expected background (with the corresponding statistical errors) and the efficiencies for Higgs masses of 50 GeV/c^2 and 100 GeV/c^2 (with 1-2% of statistical error).

5.3 Two photons and missing energy

All purely photonic candidate events were allowed to have at most 5 good charged particle tracks, none of them associated to VD track elements or to signals in the muon cham-

bers. Charged particle tracks not associated to energy deposits above 5 GeV had to have momenta below 5 GeV/c and the minimum transverse energy between any two particles reconstructed in the same hemisphere had to be greater than 5 GeV.

Cosmic-rays crossing the detector outside the tracking devices and leaving only energy deposits in the calorimeters are an important source of background for final states with photons and missing energy. Most cosmic-ray events crossing the tracking system were removed by requiring the impact parameters of all charged particle tracks to be below 4 cm in the transverse plane and below $4\text{cm}/\sin\theta$ in the beam direction. The remaining cosmic-ray events were vetoed requiring that the sum of the energies of the unassociated neutral objects was less than 10% of the energy of the reconstructed particles. Moreover, the hadronic energy associated to each photon was required to be less than 98% of its total energy and the direction of photons reconstructed in the HPC was required to be consistent within 25° with the hypothesis that the particle was coming from the primary vertex.

After this preselection, only events with two photons reconstructed above 25° and well contained either in the FEMC or in the HPC (excluding polar angles between 35° and 42°) were kept.

The main background process for this channel is the production of $\nu\bar{\nu}$ pairs (either through Z^0 or $W^{\pm}$ boson exchange) along with the emission of ISR photons. Even if the cross-section is low these events constitute an irreducible source of background. The background from the QED reaction $e^+e^- \to \gamma\gamma(\gamma)$, which has a large cross-section, were dramatically reduced by appropriate kinematic requirements. Most QED events can be vetoed by imposing that the angle between the two photons was less than 178° and that the energy of the most energetic photon was below $0.4\sqrt{s}$. Additional criteria were applied to events with photons falling in the less efficient regions of the electromagnetic calorimeters. If one of the photons was either within 1.5° of an azimuthal modular division of the HPC, or if its polar angle corresponded to the HPC edges, (defined by the intervals $[42°, 44°]$ and $[87°, 88°]$), the acoplanarity[2] was required to be above 3° and 5°, respectively. If there was one converted photon in the FEMC, the acoplanarity cut at 3° was also applied, in order to account for the larger deflection of charged particles in the forward region. In order to eliminate events with a third unseen photon, it was also imposed that any signals observed in the 40° hermeticity counters were within 20° of a reconstructed photon.

A kinematic fit was then performed imposing the Z^0 mass on the invisible system, after requiring that the missing mass of the selected event was larger than 20 GeV/c^2. The total $\chi^2/ndof$ resulting from the fit was required to be below 5.

The results of the selection in the year 2000 data set are summarized in table 4, where the SM expectations were corrected for trigger efficiencies [3]. The invariant mass spectra in last selection level is shown in figure 2, and the corresponding numbers of selected events in each data set are given in table 5.

[2]The acoplanarity between two objects is defined as the complementary, with respect to 180°, of the angle between them in the plane transverse to the beam direction.

[3]In the other channels the effect of trigger efficiencies is negligible with respect to the statistical errors on the expectations.

Selection	Data	Background	QED	$\nu\bar{\nu}\gamma\gamma$	eff_{50}	eff_{100}
preselection	1077	1121.2 $\pm$7.9	1110.6 $\pm$7.9	10.6 $\pm$0.8	60%	64%
2 γs : $\theta_\gamma \notin [35°, 42°]$	879	924.5 $\pm$7.2	915.7 $\pm$7.1	8.8 $\pm$0.7	50%	56%
$\alpha_{\gamma\gamma} < 178°$	206	200.0 $\pm$3.3	191.2 $\pm$3.2	8.8 $\pm$0.7	50%	56%
QED veto	13	9.0 $\pm$0.7	1.2 $\pm$0.3	7.8 $\pm$0.7	48%	53%
Z_{fit}	6	6.6 $\pm$0.6	0.5 $\pm$0.2	6.1 $\pm$0.6	44%	50%

Table 4: $h^0Z^0 \to \gamma\gamma\nu\bar{\nu}$ selection in the year 2000: the evolution of the data sample with the analysis cuts is shown, together with the total expected background (and to the QED and $\nu\bar{\nu}\gamma\gamma$ expectations) and corresponding statistical errors. The efficiencies for Higgs masses of 50 GeV/c^2 and 100 GeV/c^2 are shown in the last two columns, and have associated statistical errors of 1-2%.

5.4 Results on h^0Z^0 production

A good agreement between data and SM expectations was found in all analysed channels, with a total of 54 events selected and 52 $\pm$1 expected. The detailed numbers per channel and centre-of-mass energy are shown in table 5.

$\sqrt{s}$	$\mathcal{L}$	$q\bar{q}\gamma\gamma$		$\nu\bar{\nu}\gamma\gamma$		$l^+l^-\gamma\gamma$	
(GeV)	(pb^{-1})	DATA	MC	DATA	MC	DATA	MC
183	49	4	2.64 $\pm$0.12	2	1.59 $\pm$0.65	–	–
189	153	8	6.85 $\pm$0.33	5	4.82 $\pm$0.55	1	1.70 $\pm$0.44
192	26	0	1.17 $\pm$0.05	1	0.93 $\pm$0.13	0	0.27 $\pm$0.07
196	77	4	3.24 $\pm$0.15	2	2.29 $\pm$0.26	2	0.62 $\pm$0.15
200	85	4	3.15 $\pm$0.15	2	2.31 $\pm$0.24	0	0.60 $\pm$0.15
202	42	3	1.66 $\pm$0.08	1	0.99 $\pm$0.15	0	0.25 $\pm$0.07
205	78	3	3.13 $\pm$0.10	2	2.40 $\pm$0.29	0	0.61 $\pm$0.16
206.5	55	3	2.20 $\pm$0.10	4	1.58 $\pm$0.22	0	0.29 $\pm$0.07
207	84	3	3.11 $\pm$0.14	0	2.58 $\pm$0.31	0	0.69 $\pm$0.17
TOT	647	32	27.15 $\pm$0.38	19	19.49 $\pm$1.06	3	5.03 $\pm$0.55

Table 5: Selected data for h^0Z^0 production and corresponding background expectations for the three topologies and all data samples considered. The errors on the background are statistical only.

Limits on the production cross-section of h^0Z^0 with $h^0 \to \gamma\gamma$, as a function of M_{h^0}, were obtained by combining all the channels and centre-of-mass energies using the Modified Frequentist Likelihood Ratio method [16] taking into account the measured and expected mass distributions.

The signal samples generated with Pythia 6.1 were cross-checked with a dedicated generator HZHA [17] and found to be compatible within the statistical uncertainty of 1%. Different fragmentation/hadronization models were also compared, and found to have

negligible impact in the $q\bar{q}\gamma\gamma$ selection. Extra systematic effects could come from the parameterization of the background, and namely the invariant $\gamma\gamma$ mass distributions in data and background. All these effects were found to be small in comparison to the statistical uncertainty on the background expectations. To account for all effects, a systematic error of 3% was assigned to the signal efficiency used in the limit calculation.

Figure 3 shows the 95% Confidence Level (CL) lower limit on the ratio of the h^0Z^0 production cross-section to the SM one, multiplied by $BR(h^0 \to \gamma\gamma)$, as a function of the Higgs boson mass. This ratio is equal to $\sin^2\delta$ in 2HDM. For the range of masses studied, and taking the model in [2] as a reference, the width of the Higgs boson is always below the mass resolution of the analyses.

In a model where the Higgs couplings to bosons have SM values, but the couplings to fermions vanish, a 95% CL mass limit is given by the intersection of the cross-section limit and the BR prediction of the model at 104.1 GeV/c^2, while the expected limit would be of 104.6 GeV/c^2.

6 Search for h^0A^0 Production

6.1 $\mathbf{A^0 \to b\bar{b}}$

The analysis of the $b\bar{b}\gamma\gamma$ final state is very similar to that of $h^0Z^0 \to q\bar{q}\gamma\gamma$. Most of the selection was kept except for the fit imposing the Z^0 mass. In the h^0A^0 case less constraints were used: the jet-jet invariant mass was left free and an additional ISR photon was allowed in the beam direction. In fact, if $M_{h^0} + M_{A^0} < M_{Z^0}$, a significant part of the signal events may correspond to radiative returns to the Z^0 with subsequent $Z^0 \to h^0A^0$. Since M_{A^0} has to be fitted without constraints, the global $\chi^2/ndof$ becomes an important selection criterion: in addition to the previous partial $\chi^2/ndof$ cuts, the global $\chi^2/ndof$ was required to be below 10 in all cases.

In the next stage, it was required that $|E_{\gamma 1} - E_{\gamma 2}| < 0.70|E_{\gamma 1} + E_{\gamma 2}|$. Again, at least one of the photons had to be in the HPC and, in a final level, the combined b-tagging of the event, as defined in [18], was required to be above -2. Figure 4 shows the agreement of the b-tagging variable in data and SM simulation, together with the mass distributions obtained for h^0 and A^0.

Selection	Data	Background	$q\bar{q}$	eff_{100}
no-ISR/FSR	88	72.6±0.8	67.8±0.5	53%
fit	74	64.1±0.7	61.1±0.5	49%
ΔE	61	55.7±0.7	52.7±0.4	49%
HPC	59	53.8±0.6	50.9±0.4	49%
b-tag	21	22.8±0.4	21.4±0.2	46%

Table 6: $h^0A^0 \to \gamma\gamma b\bar{b}$ analysis: the comparison of data and MC events selected in each analysis level for all data. The $q\bar{q}(\gamma\gamma)$ contribution is shown separately. The efficiency for the selection of a h^0A^0 signal with $M_{h^0} = 100$ GeV/c^2 and $M_{A^0} = M_{Z^0}$ produced at $\sqrt{s}$=206 GeV is shown in the last column (the corresponding statistical errors being of 1-2%).

The total numbers of data and background selected in the analysis are shown in table 6. The non-$q\bar{q}$ background is larger compared to the case with the Z^0 mass constraint: it consists mainly of semi-leptonic W^+W^- events, in which the electron was reconstructed as two separate neutral clusters, with invariant mass ~ 0. The table shows also the efficiency obtained for $e^+e^- \to h^0A^0$ with $M_{A^0} = M_{Z^0}$ and $M_{h^0} = 100$ GeV/c^2.

6.2 $\mathbf{A^0 \to h^0 Z^0}$

When kinematically allowed, the decay $A^0 \to h^0Z^0$ is the dominant one for a large range of parameters. This will lead to final states with a fermion pair and four photons. Only the Z^0 decay to quark pairs, which has the highest branching ratio, was analysed. At least three isolated photons were required, with at most one conversion.

At least two of the photons had to be above 30° in polar angle and have a transverse energy in respect to any of the jets greater then 7.5 GeV. No fit was performed but the jet-jet invariant mass was required to be in the range 50 to 130 GeV/c^2. The difference between the energy of any of the photons and the energy carried by all the others had to be below $0.33E_{ret}$. In the last selection level, one of the photons was required to be in the HPC, and at least three photons were required to be above 15° in polar angle.

The number of events selected in all data samples and the corresponding SM expectations are given in table 7. The efficiencies for the signal are as high as 60% for high masses, and are above 40% for most of the considered range. Since only three photons are required, no mass reconstruction was attempted and the result is based on the number of events selected at this stage.

Selection	Data	Background	$q\bar{q}$
no-ISR/FSR	16	13.7 ±0.3	13.1 ±0.3
Z^0 mass	10	10.3 ±0.3	9.7 ±0.3
ΔE	5	5.9 ±0.2	5.4 ±0.2
HPC	3	2.7 ±0.2	2.4 ±0.1

Table 7: $h^0A^0 \to q\bar{q}\gamma\gamma\gamma(\gamma)$ analysis: the comparison of data and MC selected in each analysis level for all data is shown. The error on the MC is statistical only.

6.3 Results on h^0A^0 production

Within the framework of general 2HDM, the main decay channel of A^0 is $b\bar{b}$ for a wide range of parameters, but the decay to h^0Z^0 becomes dominant when kinematically allowed.

Limits were extracted with the same algorithm as for h^0Z^0. In the $b\bar{b}\gamma\gamma$ channel the reconstructed mass values were used, while for the $q\bar{q}\gamma\gamma\gamma(\gamma)$ there was no attempt to reconstruct the masses, which reduces this channel to a pure counting experiment. Both channels had similar performance.

To extract upper limits on $\cos^2\delta$, reference cross-sections computed with [17] were used. For the $h^0 \to \gamma\gamma$ decay, the BR computed with $\sin^2\delta = 1$ and shown in figure 3 was used, representing a conservative assumption since BR($h^0 \to \gamma\gamma$) increases for lower

$\sin^2\delta$. Depending on the point in parameter space under consideration, the limit was derived from the dominant decay channel of the A^0 ($b\bar{b}$ or h^0Z^0) which was assumed to have 100% BR.

Figure 5 shows the limits on $\sin^2\delta$ obtained for two different M_{A^0} values as a function of M_{h^0}. As mentioned above, these limits strongly depend on the mass hypothesis used for h^0 and A^0.

7 Exclusion in the 2HDM parameter space

The combination of the results on h^0Z^0 and h^0A^0 production, is illustrated in figure 5. The upper limits on $\sin^2\delta$ for a given M_{h^0} and the upper limits on $\cos^2\delta$ for a given (M_{h^0},M_{A^0}) pair are combined to exclude the (M_{h^0},M_{A^0}) pair for all δ values.

Figure 6 shows the 95% CL exclusion in the plane (M_{h^0}, M_{A^0}) divided in separate regions according to the different kinematics:

I. $M_{A^0} > M_{h^0} + M_{Z^0}$

The main decay channels in this region are $h^0 \to \gamma\gamma$ and $A^0 \to h^0Z^0$ and the $\gamma\gamma Z^0$ and $q\bar{q}\gamma\gamma\gamma(\gamma)$ channels are the relevant ones. The vertex $A^0h^0Z^0$ is proportional to $\cos\delta$ and thus, the decay $A^0 \to h^0Z^0$ is dominant only for $\sin^2\delta < 0.95$. However, above this value the mass combinations are excluded by the limits on h^0Z^0 production.

II. $M_{h^0}/2 < M_{A^0} < M_{h^0} + M_{Z^0}$

Most of the parameter space region is dominated by $h^0 \to \gamma\gamma$ and $A^0 \to b\bar{b}$. However, the decay $A^0 \to b\bar{b}$ is suppressed as $\sin^2\delta$ approaches 0, and the A^0 becomes invisible for $\sin^2\delta < 10^{-6}$, while the exclusion in this region depends on the search for hA production. For that particular case, the results of a $\gamma\gamma + E_{mis}$ analysis (described in [3]) are used. They cover all the exclusion region obtained from the combination of the h^0Z^0 and $b\bar{b}\gamma\gamma$ analyses for higher $\sin^2\delta$ values. The exclusion shown in figure 6 is thus valid for all δ.

III. $2M_b < M_{A^0} < M_{h^0}/2$

Complementary to $A^0 \to h^0Z^0$, also $h^0 \to A^0A^0$ becomes dominant when kinematically allowed. The A^0 still decays to $b\bar{b}$ if kinematically allowed, and this gives rise to 6-fermion final states. This decay is relevant for most 2HDM, and we refer to the study published by DELPHI in [6]. For very low $\sin^2\delta$ there will then be a region of totally invisible final states for which the results on the invisible Z^0 width are the only available experimental information. Results from LEP1 are then used, as explained in [3].

The LEP1 results on the total Z^0 width (see ref. [3]) are also used to cover the region where the two masses are below the reach of the present analysis.

These exclusions are valid for all the allowed parameter space in the case of Potential A, but only for M_{H^+} >500 GeV/c^2 or $\sin^2\delta > 0.1$ in the case of Potential B. For lower values of both M_{H^+} and $\sin^2\delta$, the BR($h^0 \to \gamma\gamma$) can vanish due to cancellation of the different loop contributions.

Within the two potentials considered, the exclusions given for invisible A^0 (which are more restrictive than the ones for visible final states, in region III) apply only to small mass regions because $\sin^2\delta < 10^{-6}$ implies $M_{h^0} \sim 0$ in Potential A and $M_{h^0} \sim M_{A^0}$ in Potential B. Both bands are in principle outside region III, but since the precise width of these bands is not known, we show the corresponding region of exclusion for invisible A^0.

8 Conclusions

Around 650 pb^{-1} of LEP2 data, collected at centre-of-mass energies between 183 and 209 GeV, were analysed in the search for Higgs bosons decaying into photons. In the context of 2HDM, both h^0Z^0 and h^0A^0 production were considered, consisting on a large variety of final states involving photons and fermions. No evidence for new physics was found.

Lower limits were set on the mass of a resonance with Higgs-like couplings to bosons and decaying to two photons. Bounds were derived on the mass plane of the lightest scalar particles of the fermiophobic 2HDM scenario.

References

[1] K. Hagiwara, R. Szalapski and D. Zeppenfeld, Phys. Lett. **B318** (1993) 155;
K. Hagiwara, S. Ishihara, R. Szalapski and D. Zeppenfeld, Phys. Rev. **D48** (1993) 2182.

[2] A. Barroso, L. Brücher, R. Santos, Phys. Rev. **D60** (1999) 035005;
L. Brücher, R. Santos, Eur. Phys. J. **C12** (2000) 87.

[3] DELPHI Coll., P. Abreu *et al.*, Phys. Lett. **B507** (2001) 89.

[4] DELPHI Coll., P. Abreu *et al.*, Phys. Lett. **B458** (1999) 431.

[5] ALEPH Coll.,R. Barate *et al.*, Phys. Lett. **B487** (2000) 241;
L3 Coll., P. Achard *et al.*, Phys. Lett. **B534** (2002) 28;
OPAL Coll.,G. Abbiendi *et al.*, Phys. Lett. **B544** (2002) 44.

[6] DELPHI Coll., J. Abdallah *et al*, "Searches for Neutral Higgs Bosons in Extended Models", to be submitted to Eur. Phys. J.

[7] DELPHI Coll., J. Abdallah *et al*, "Search for Charged Higgs Bosons at LEP in general 2HDM", to be submitted to Eur. Phys. J.

[8] DELPHI Coll., P. Aarnio *et al.*, Nucl. Instr. and Meth. **A303** (1991) 233;
DELPHI Coll., P. Abreu *et al.*, Nucl. Instr. and Meth. **A378** (1996) 57.

[9] DELPHI Silicon Tracker group, P. Chochula *et al*, Nucl. Instr. and Meth. **A412** (1998) 304.

[10] T. Sjöstrand *et al.*, Comp. Phys. Comm.**135** (2001) 238.

[11] S. Jadach and B.F.L. Ward and Z.Wąs, Comp. Phys. Comm. **130** (2000) 260.

[12] S. Jadach and B.F.L. Ward and Z.Wąs, Comp. Phys. Comm. **79** (1994) 503.

[13] S. Jadach, W. Placzek and B.F.L. Ward, Phys. Lett. **B390** (1997) 298.

[14] S. Catani *et al.*, Phys. Lett. **B269** (1991) 432.

[15] DELPHI Coll., P. Abreu *et al.*, Eur. Phys. J. **C2** (1998) 581.

[16] A.L. Read, "Modified Frequentist Analysis of Search Results (The CLs Method)" in "Workshop on Confidence Limits", ed. F. James, L. Lyons and Y.Perrin, CERN Report 2000-005 (2000) p.81.

[17] P. Janot "HZHA", in "Physics at LEP2", ed. G.Altarelli, T.Sjöstrand and F.Zwirner, CERN Report 1996-001 (1996) Vol. 2, 309.

[18] DELPHI Coll., J. Abdallah *et al*, "b-tagging in DELPHI at LEP", submitted to Eur. Phys. J. C.

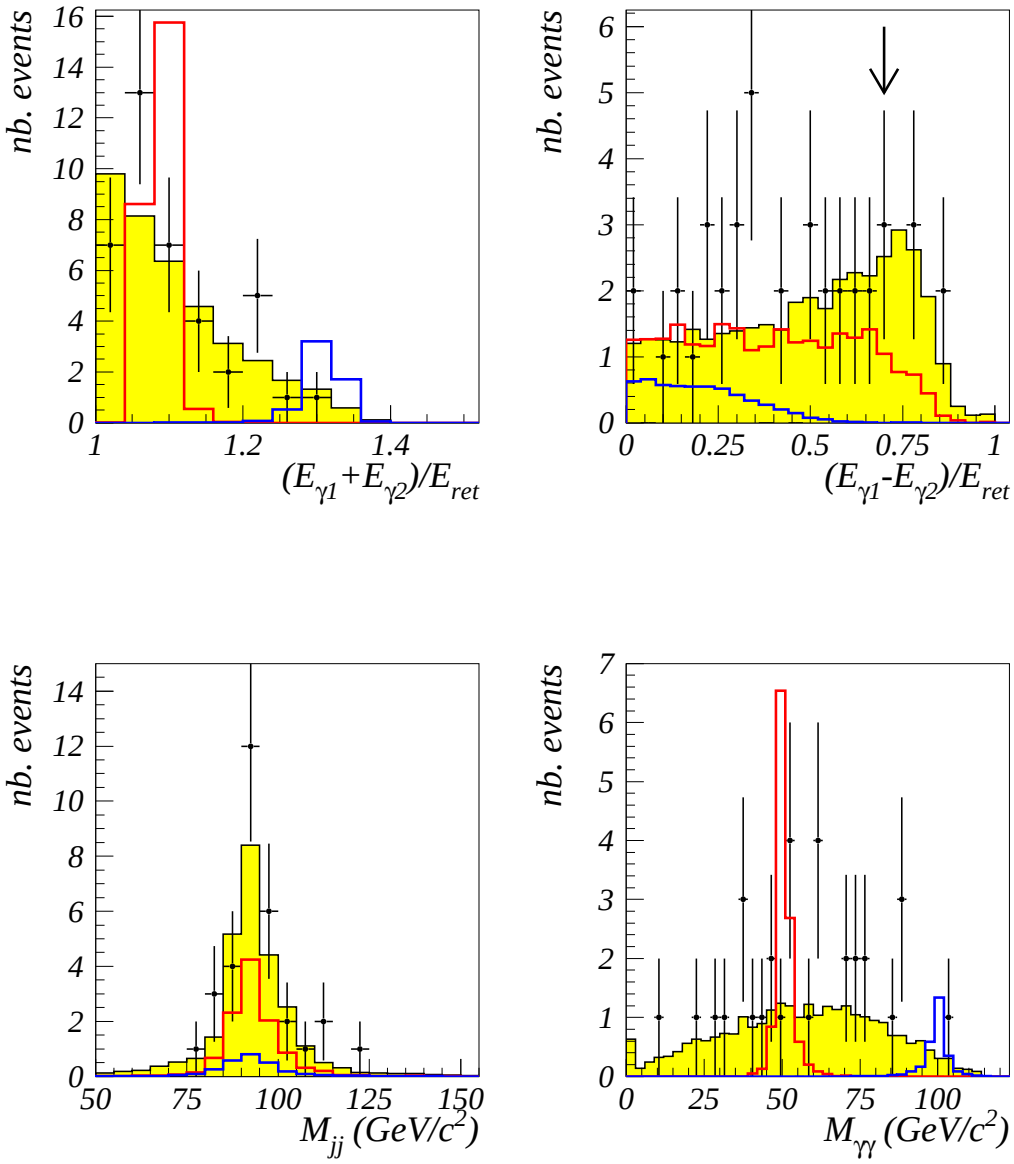

Figure 1: $h^0Z^0 \to \gamma\gamma q\bar{q}$. The top plots show the sum (left) and difference (right) of the two photon energies divided by the radiative return energy before the cut on the energy difference (indicated by the arrow). The bottom plots show the reconstructed invariant jet-jet mass (left) and the fitted Higgs mass (right). The full data set (dots) is compared to the SM background (shaded area) and two h^0Z^0 signals: with M_{h^0}=50 GeV/c^2 and M_{h^0}=100 GeV/c^2 (thick lines), shown with arbitrary normalization.

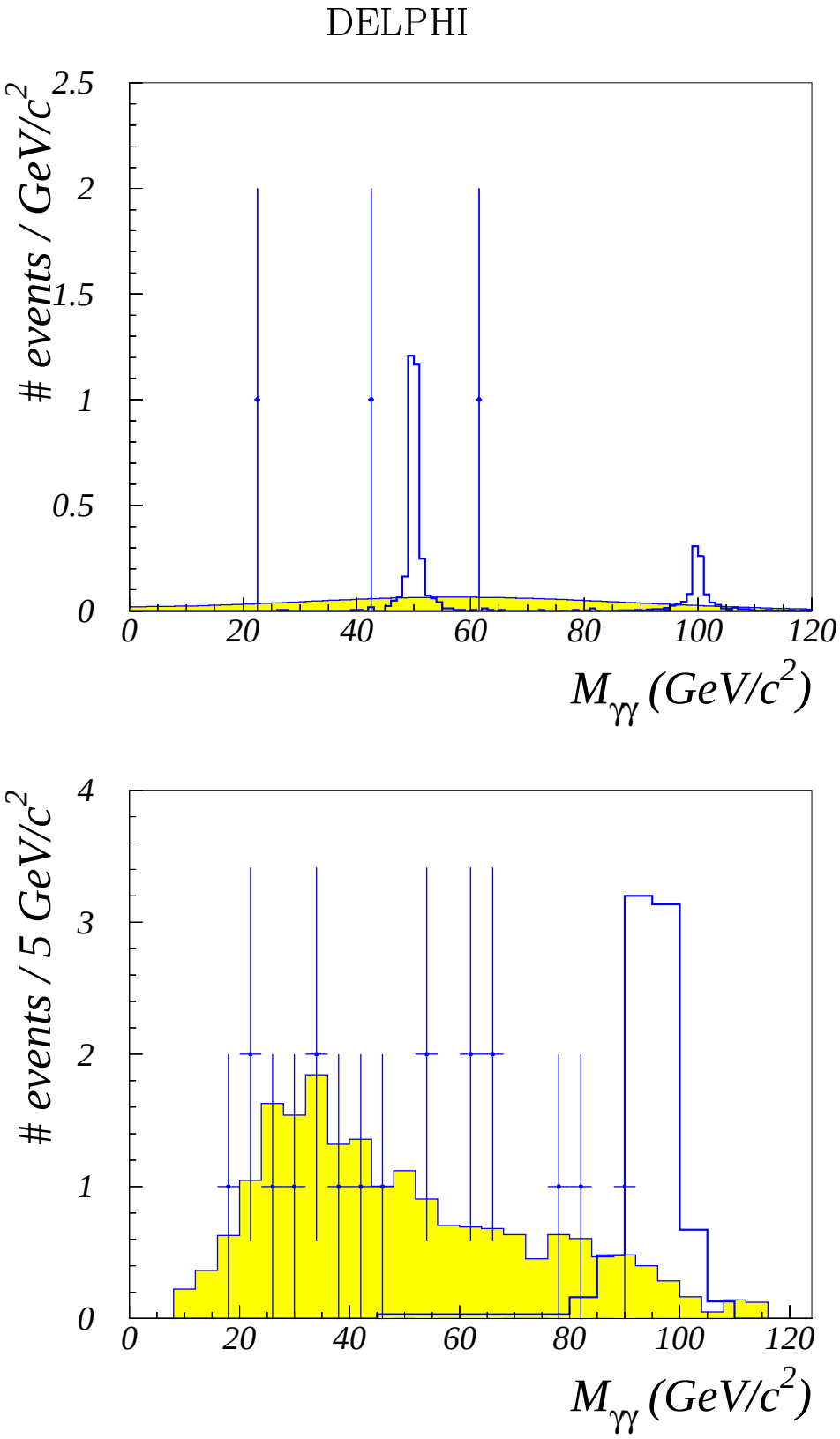

Figure 2: $h^0Z^0 \to \gamma\gamma l^+l^-$ (top) and $h^0Z^0 \to \gamma\gamma\nu\bar{\nu}$ (bottom). The invariant masses $M_{\gamma\gamma}$ at the last selection level for all analysed data (dots) are compared to the SM background expectations (shaded histogram), and h^0Z^0 signals of 50 and 100 GeV/c^2 (top) and 95 GeV/c^2 (bottom), shown with arbitrary normalization.

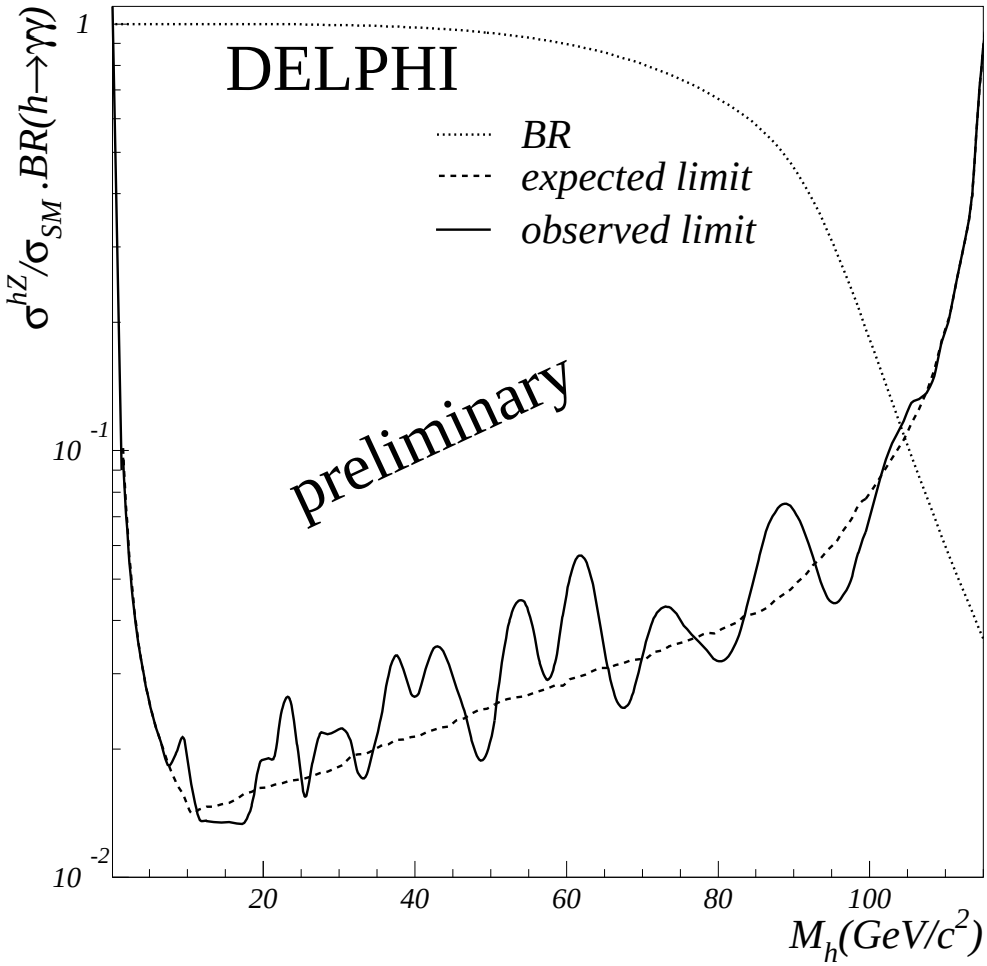

Figure 3: 95% CL limit on the h^0Z^0 production cross-section normalized to the SM value $\times$ BR($h^0 \to \gamma\gamma$). Both the observed (full line) and the expected limits (dashed line) are shown. Also shown is the fermiophobic BR (dotted line), obtained by keeping the SM couplings of the Higgs to boson pairs and setting the $h^0 f\bar{f}$ couplings to 0. A 95% CL mass limit is given by the intersection of the cross-section limit and the BR curve at 104.1 GeV/c^2 (104.6 GeV/c^2 expected).

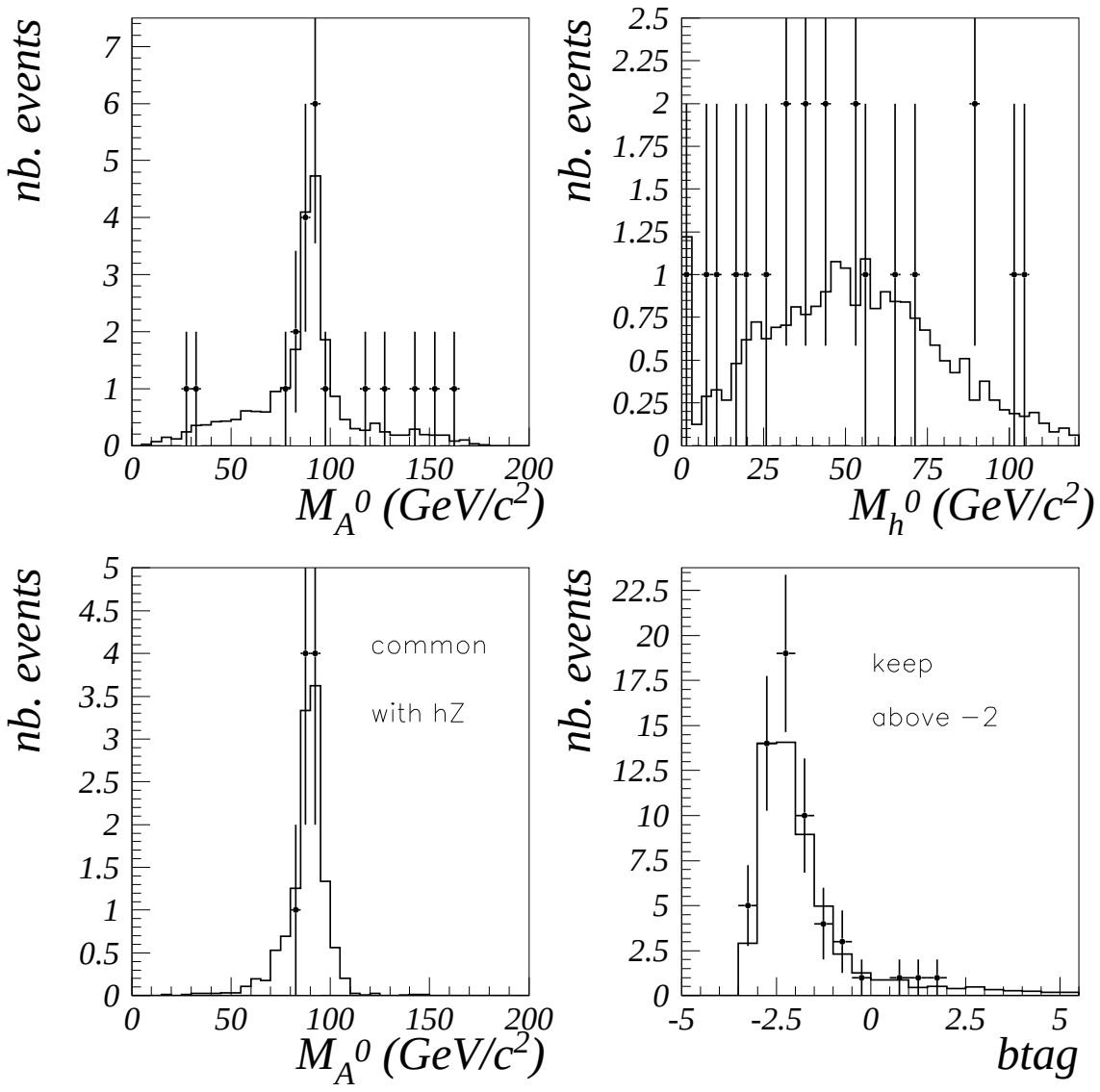

Figure 4: $h^0A^0 \to \gamma\gamma b\bar{b}$ analysis. The reconstructed A^0 and h^0 masses at the final selection level are shown in the top plots for data and expected SM background in all data sets. The lower plots show the fitted jet-jet mass for events selected in both the h^0A^0 and h^0Z^0 analyses and the distribution of the b-tag variable just before the cut at -2.

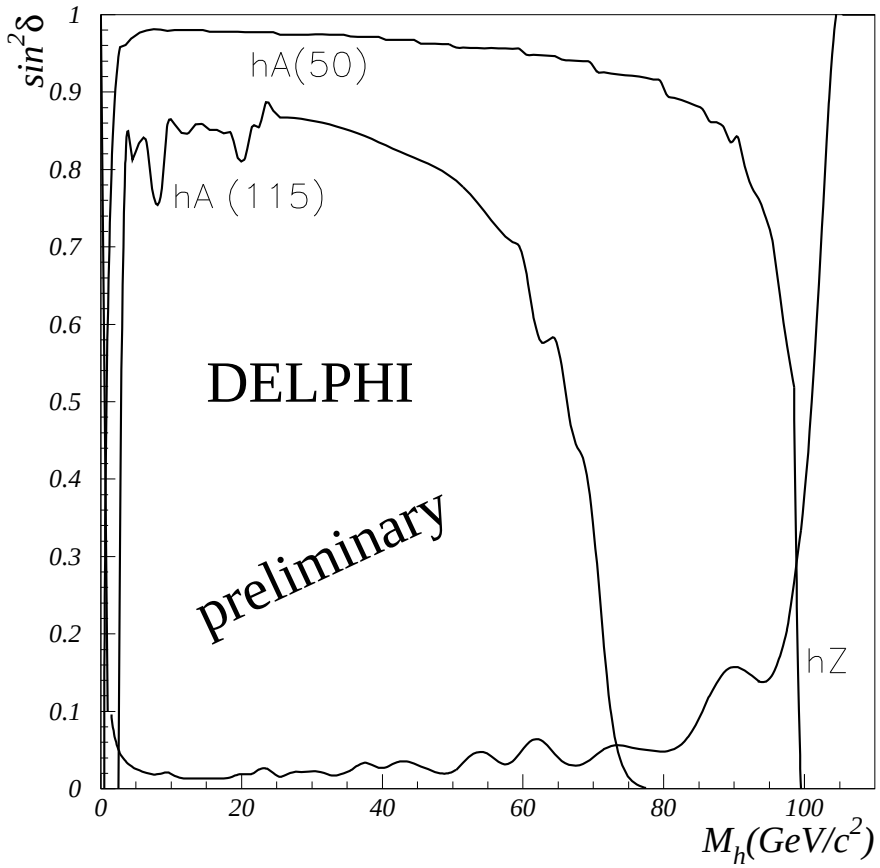

Figure 5: 95% CL limits on the h^0Z^0 and h^0A^0 production cross-sections expressed in terms of $\sin^2\delta$. Values above the h^0Z^0 curve and below the h^0A^0 curves (shown for two different M_{A^0} values: 50 GeV/c^2 and 115 GeV/c^2) are excluded.

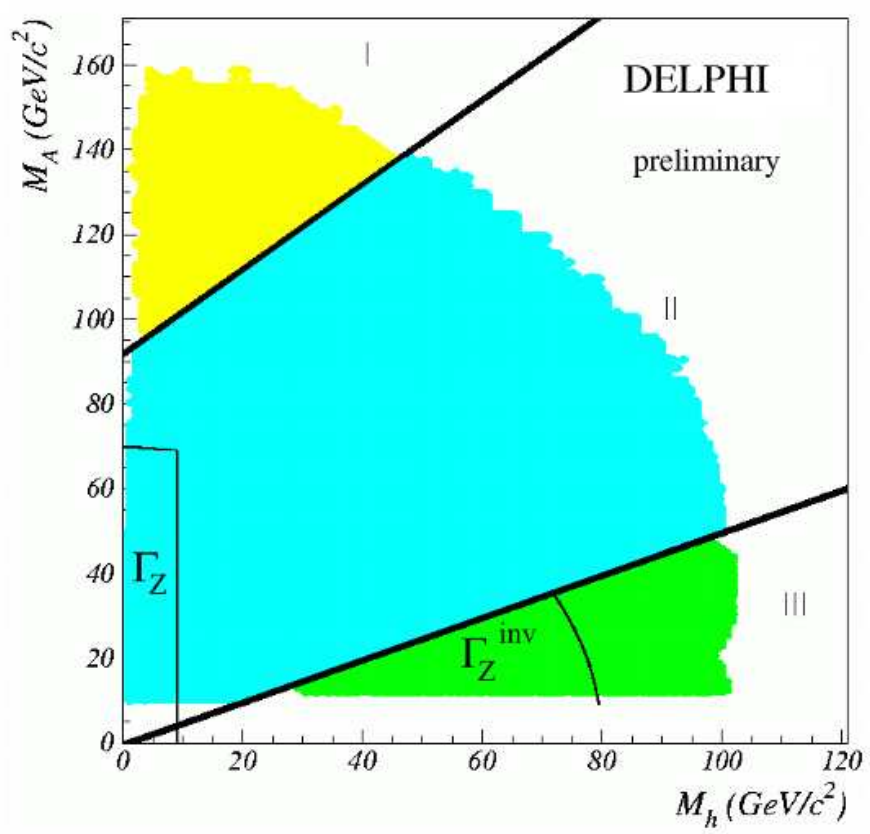

Figure 6: The shaded areas correspond to regions excluded at 95% CL for all δ values. The plot is divided in regions according to the dominant decay modes of h^0 and A^0, as explained in the text. The curves show the exclusions from LEP 1 data, based on the total and invisible width of the Z^0.